UNIVERSITY OF Cincinnati
AEROSPACE ENGINEERING
& ENGINEERING MECHANICS

SAE Aero Design® West 2004
University of Cincinnati
AeroNatiCats
Team # 029
May 7, 2004

Design Team

Dave Altherr
Terry Daviaux
Larry Kramer
Quintin Ullery
Kaiming Chen
John Davis
Tammy Prichard
Nathan Wright
Brian Croswell
Sean Halfhill
John Small

TABLE OF CONTENTS

A VERY WELL WRITTEN REPORT.

1.0 INTRODUCTION

The Society of Automotive Engineers Collegiate Design Series was created to enable students to apply the knowledge obtained in the classroom to real world problems. The Aero Design® Competition requires teams to design, build, and fly an aircraft given specific design constraints. These constraints include a maximum take-off limit of 200 ft, a minimum wingspan of 10 ft., a maximum landing distance of 400 ft, and contain a 4" x 5" x 6" minimum payload bay. In addition, the aircraft must use an OS 0.61 FX engine fueled with 10 % nitro-methane fuel. The main objective is to lift the most weight possible following the design constraints. The aircraft must also be radio-controlled and piloted by an AMA licensed pilot.

To accomplish the task of creating an aircraft to meet the design criteria, the design team was divided into several groups, each performing specific tasks. The layout group's main responsibilities were to create all the drawings for construction and competition. The aerodynamics group's responsibilities included airfoil selection, estimating drag polars, and calculating L/D. The structure, weight and balance group performed all structural calculations including the wing build-up, wing spar, and placed the main components to balance the aircraft at a set center of gravity location (CG). The propulsion group conducted engine testing to determine the engine operating conditions. The stability and controls group calculated static stability derivatives and performed dynamic analysis to validate the design. The performance group's main task was to calculate all aircraft performance quantities such as ground roll distance, rate of climb, and available thrust. Finally, the optimization group performed iterative calculations using the MathCAD models produced by each of the aforementioned design groups to determine an optimal configuration. Each group's results are discussed in the following sections.

2.0 LAYOUT

The layout of the aircraft design was chosen to be that of a conventional aircraft due to the simplicity of construction and ease of calculations. A double tapered wing was chosen for ease of construction and its

close approximation to an optimal elliptic lift distribution. The length of the tail boom was determined by using a tail volume coefficient of a general aviation aircraft close to the current design. The overall length of aircraft was determined by setting a center of gravity and calculating the weights required to balance the aircraft. This is discussed in further detail in section 4.0.

The attached drawings show the aircraft configuration and pertinent dimensions for the wing, vertical tail, horizontal tail, and fuselage. All dimensions shown in the drawings are for the final design configuration. Five drawings were chosen to best describe the design. A three view drawing showing the major aircraft dimensions is shown in Sheet 1 of the attached drawings. The component area dimensions are also shown in tabular form in Sheet 1. A skid plate can be seen attached to the rear fuselage. This skid plate is used to limit the aircraft rotation at liftoff such that over-rotation is avoided which would result in lift off at a velocity lower than that needed for sustained flight. Sheet 2 shows a structural isometric view depicting the internal structure of the aircraft. A detailed drawing of the main wing structure is shown in Sheet 3 while the fuselage structure is shown in Sheet 4. The connection points for the forward and rear fuselage break-away sections can be seen in the exploded view in Sheet 4. The last drawing (Sheet 5) shows the structural details of the vertical and horizontal tail.

3.0 AERODYNAMICS

Since the aircraft configuration is of a conventional design the aerodynamics of this configuration are relatively straight-forward. The major points of the aerodynamic analysis included the selection of an airfoil for the main wing, airfoil selection for the horizontal and vertical tail, and lift and drag calculations for entire aircraft at trimmed flight conditions. All calculations for the aerodynamic analysis were performed in a static MathCAD model giving the ability for the calculated aerodynamic quantities (lift, drag, max lift over drag, etc.) to be easily passed to other analysis models such as performance, stability, controls, etc. Each area of the aerodynamic analysis is discussed in full detail in the following subsections.

3.1 Airfoil Selection

Several high lift, low Reynolds Number airfoils were investigated. Many of these airfoils have high moment coefficients which are not desirable since this would require a higher counter moment from the tail to stabilize the aircraft. Therefore, the Drela DAE11 airfoil was chosen since it provided high lift (maximum lift coefficient equal to 1.6) at low Reynolds Numbers with only a moderate moment coefficient of approximately -0.12. The drags of the airfoils under investigation were all relatively equal, thus, although the drag is important in the aerodynamics analysis it is not a factor in airfoil selection. The DAE11 airfoil is shown in Figure 3.1.

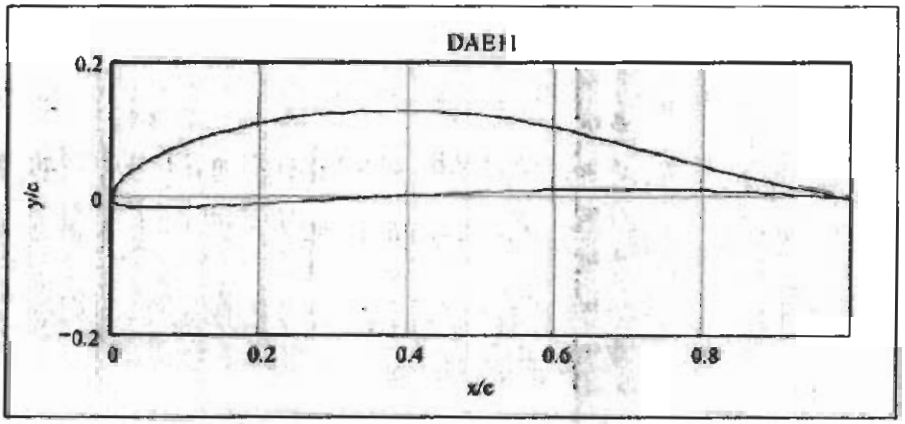

Figure 3.1: Drela DAE11 Airfoil

Figure 3.2 shows the main wing drag polar. The airfoil 2D section data and the induced drag effects on the wing are plotted in Figure 3.2 as separate curves to show their contributions to the overall main wing drag polar. The solid red line in Figure 3.2 represents the total wing drag while the dotted blue line shows the 2D section data and the dashed black line is representative of the induced drag effects. It can be seen that the induced drag has a drastic effect on the overall main wing drag at high lift coefficients while at the lower lift coefficients (representative of low angles of attack) the induced effects are smaller and the overall wing drag more closely matches the 2D section data.

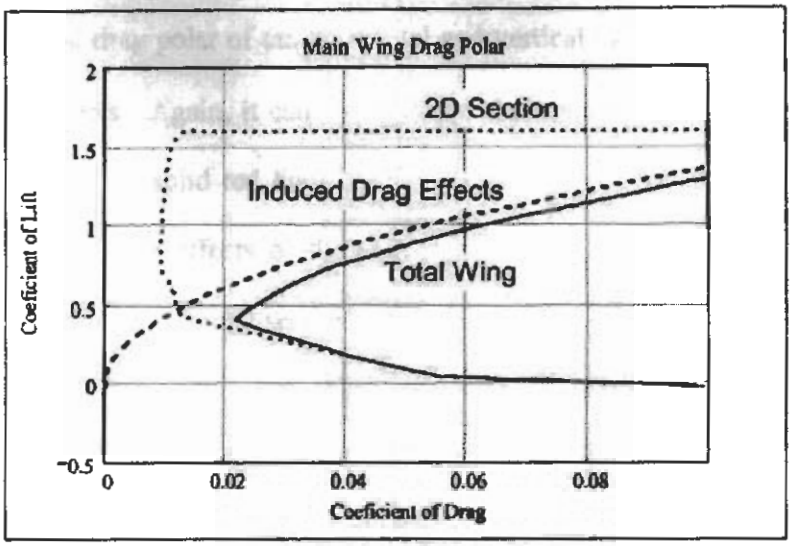

GOOD POLAR

Figure 3.2: Main Wing Drag Polar

The NACA 0009 was chosen for the horizontal and vertical tail due to its low drag performance over a wide range of attack angles (wide drag bucket) at the required low Reynolds numbers. It was thought that after the design was closer to final, the horizontal tail airfoil could be changed such that the horizontal tail at zero incidence would balance the moments generated by the main wing at lift off conditions, namely an airspeed of 1.2 times the stall speed of the aircraft. For the final design the long tail provided a long moment arm thus the lift required by the horizontal tail to balance the aircraft was relatively small and could easily be accounted for in a small downward incidence of the symmetric horizontal tail. This incidence only needed to be approximately 0.3 degrees downward to balance the aircraft at lift off conditions. Therefore, the NACA 0009 was kept as the airfoil configuration of the horizontal tail. The NACA 0009 2D section profile is shown below in Figure 3.3.

Looks like Drag was a consideration in these airfoils.

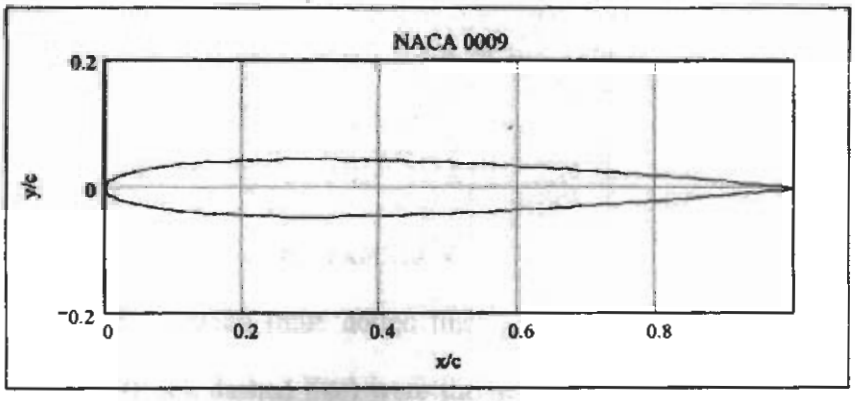

Figure 3.3: NACA0009 Airfoil

Figure 3.4 shows the total drag polar of the horizontal and vertical tail plotted with the 2D section data and the induced drag effects. Again, it can be seen that the induced drag effects (dashed black line) shaped the overall drag polar (solid red line). However, since the airfoil used for the horizontal and vertical tail was symmetric the effects of the induced drag are symmetric. The wide drag bucket mentioned earlier can be seen in the 2D section data (blue dotted line) in Figure 3.4. Since the airfoils chosen for both the horizontal and vertical tail were identical the drag polar shown in Figure 3.4 is equally representative of each tail configuration.

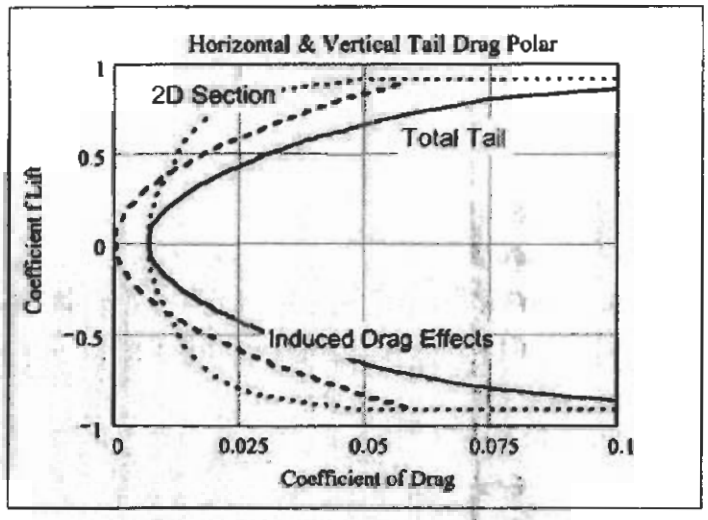

Figure 3.4: Horizontal and Vertical Tail Drag Polar

3.2 Total Aircraft Aerodynamics

The total aircraft lift and drag consists of a combination of the contributions of each component of the aircraft. The main contributors used were the main wing, horizontal and vertical tails, fuselage, and landing gear. The drag of these components was added using the "D/q" method to estimate the total aircraft drag. Figure 3.5 shows the drag build up of each of these components against the aircraft angle of attack at trimmed flight conditions. Trimmed conditions involve the elevator deflection required at each angle of attack (AOA) to balance the moment of the aircraft. It can be seen that the two highest drag components are the main wing (blue dotted line) and horizontal tail (red dot-dash line). The fuselage and landing gear (black dashed line) were the next highest contributors with the vertical tail

(magenta dashed line) giving the lowest drag contribution. It can be seen that the minimum total aircraft drag occurs at an aircraft angle of attack of approximately -0.75°. It is important to note that the drag build-up shown in Figure 3.5 is plotted against the AOA of the aircraft, which is not necessarily the AOA of each of the components. Performance points are shown on Figure 3.5 labeling the maximum climb AOA, the maximum lift over drag AOA, the lift off AOA, and the stall AOA for the trimmed aircraft.

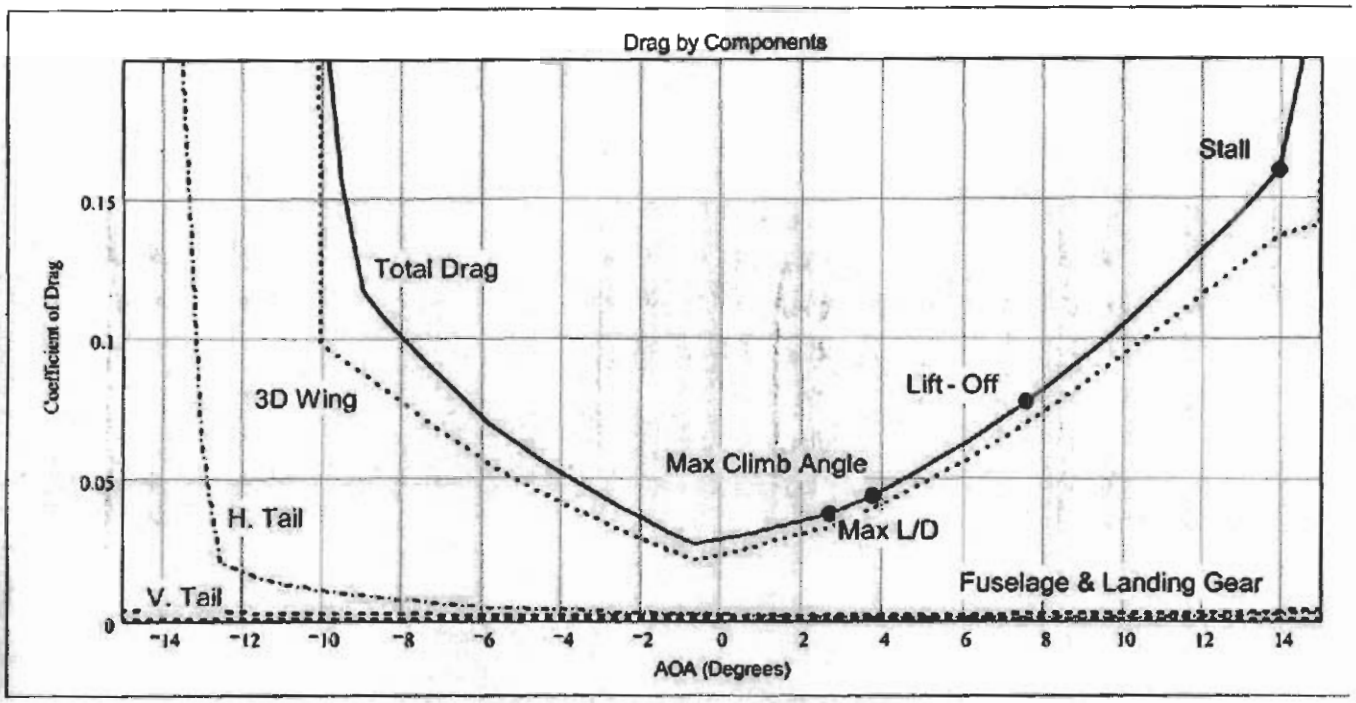

Figure 3.5: Aircraft Drag Build-Up, Trimmed Conditions

The total aircraft drag polar is shown in Figure 3.6. The three curves in Figure 3.6 represent the total aircraft drag at untrimmed flight conditions (red solid line), trimmed flight conditions (solid blue line), and the main wing effects (dotted black line). From this figure it can be seen that the effect of the deflection of the elevator constricts the drag polar at the high and low lift extremes. This is intuitive since a larger elevator deflection is needed in these flight regimes to balance the aircraft moment. Also, the close proximity of the main wing polar to the trimmed and untrimmed polars re-iterates the fact that

the main wing is the largest contributor to the lift and drag of the aircraft. Again the same four performance points described above for Figure 3.5 are shown in Figure 3.6.

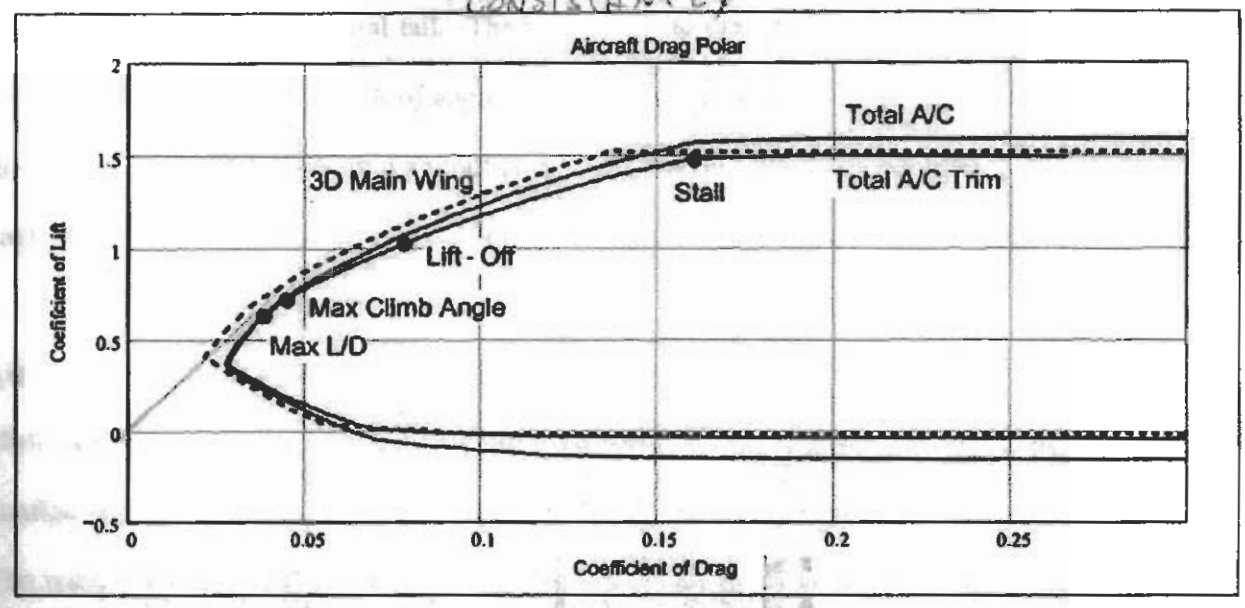

Figure 3.6: Aircraft Drag Polar

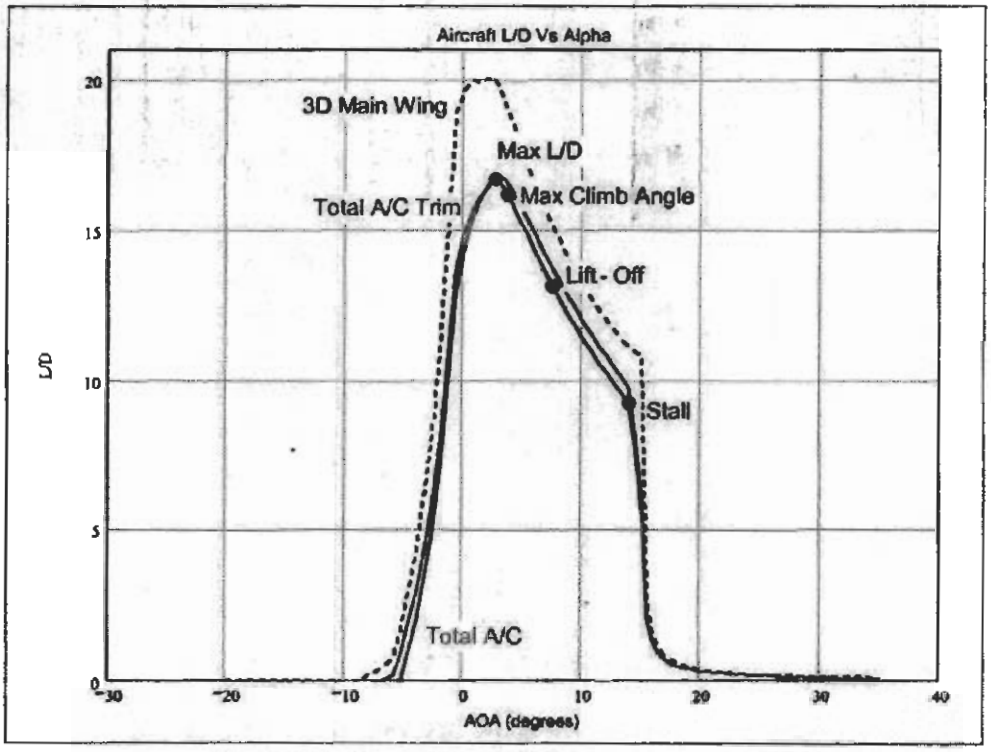

Figure 3.7: Aircraft Drag Polar and Lift over Drag

The lift to drag ratio for the same three cases (untrimmed, trimmed aircraft, and wing alone) shown in Figure 3.6 is plotted as a function of the AOA of the aircraft in Figure 3.7. Again the effects of the

elevator deflection can be seen by comparing the untrimmed data to the trimmed data. The trimmed drag curve has a slightly lower lift to drag ratio than the untrimmed polar due to the negative lift and increased drag on the horizontal tail. The highest lift to drag ratio has a value of approximately 16.6 which occurs at an aircraft AOA of approximately 3°. Also noteworthy is the large difference between the main wing curve and the total aircraft curves. This shows that despite the main wing being the main contributor to most aerodynamic quantities, the other aircraft components cannot be ignored.

4.0 STRUCTURES, WEIGHTS, AND BALANCE

Well established construction methods are used for this design, which include a standard D-spar/rib configuration for all of the lifting surfaces as well as a stringer/bulkhead configuration for the fuselage. The main landing gear is fabricated using spring-steel and is attached directly to the main wing spar running through the fuselage. The controlling idea behind the structural design is to minimize load path complexity and thus facilitate the use of the largest load bearing members with the least amount of added support structure. Skeletal representations of these techniques are shown in the attached drawings. Analytical and experimental analyses were utilized in making the various design decisions and are presented in the following subsections.

4.1 Analytical Testing for Main Landing Gear

The landing gear is a tricycle configuration using spring steel struts. The main gear is assumed to absorb a majority of the loading and therefore a theoretical deflection prediction is required for clearance purposes during landing. The main gear is oriented in such a way as to allow for roughly one and a half inches of deflection at design weight in an attempt to decrease landing impact. Deflection during landing is plotted as a function of payload weight in Figure 4.1 and is determined using dynamic loading approximated as twice the total weight. The singular point in Figure 4.1 represents the payload weight design condition but is extended for various payloads corresponding to a projected upper limit as well as the minimum eight pound capacity. Given this indicated deflection, the corresponding bending

slightly optomistic, but steel bends. Not a bad design condition given the objectives.

stress comes within five percent of the considered yield for spring steel which ultimately validates this particular construction method and material choice.

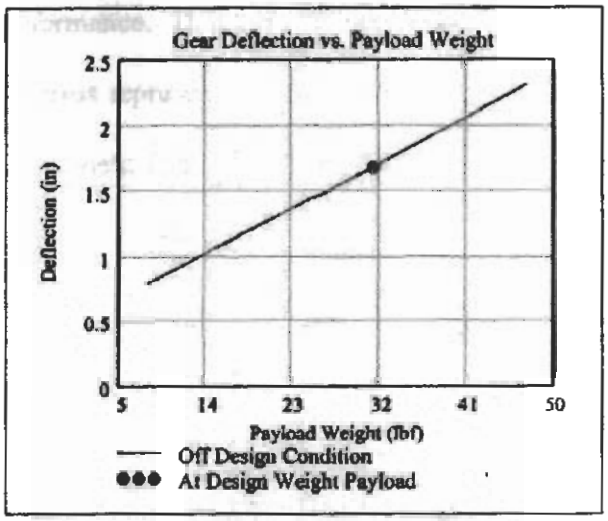

Figure 4.1: Gear Deflection at Various Payloads

4.2 Analytical Testing for Main Wing Spar

Along with the landing gear, the main wing spar was analyzed given various configurations and construction techniques in an attempt to optimize its design. Two designs were considered; a carbon tubular spar located at the quarter chord of the main wing and a wooden D-spar with the web located at the maximum airfoil thickness. The bending stress for each of the two configurations is calculated and compared with known yield values for the given material. The loading distribution is approximated using the Shcrenk approximation and is assumed to be applied directly on the spar (neglecting wing twist). Given these assumptions, this particular loading distribution is shown in Figure 4.2 accompanied by the corresponding moment and shear distributions. Main concern was placed on cantilever bending and the associated fuselage side-of-body bending stress, therefore the considered design requirement consists of not exceeding yield stress at the wing root.

Given the large wingspan considered, a three-section wing was incorporated into the design, which detaches at 55% of the semi-span. Taking advantage of this imposed sectioning of the wing, given the

tapered loading distribution, a weaker outer spar section is used to conserve weight. For the carbon spar, a smaller diameter outer tube of the same material was considered while the I-beam incorporates a weaker material to dictate performance. The results for the wooden spar are shown in Figure 4.3 where the discontinuity in the yield stress represents the material change from fir to balsa. Although there is only a 19% difference between yield and side of body stress, compared to the carbon spar, there is approximately 13% decrease in overall weight. Given this savings in weight, as well as the availability of materials and well-established construction methods, the wooden D-spar is chosen over the carbon tube.

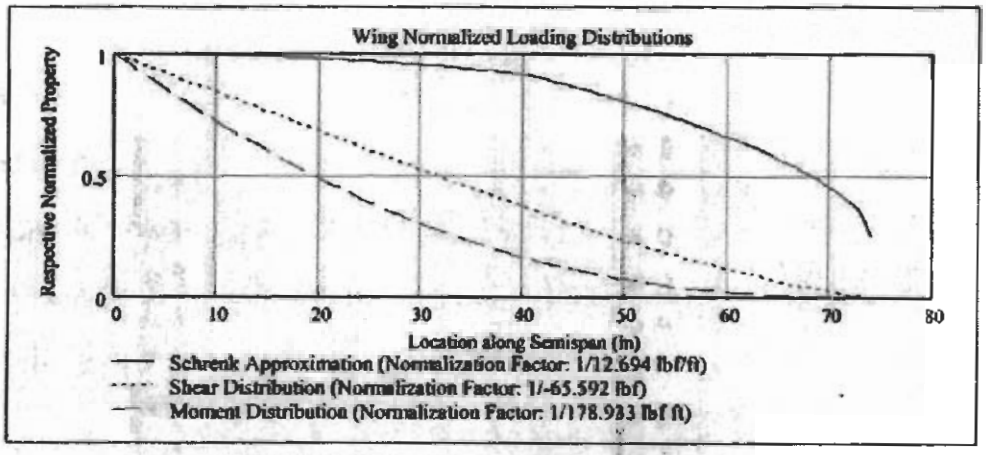

Figure 4.2: Main Wing Spar Approximated Loading Distributions

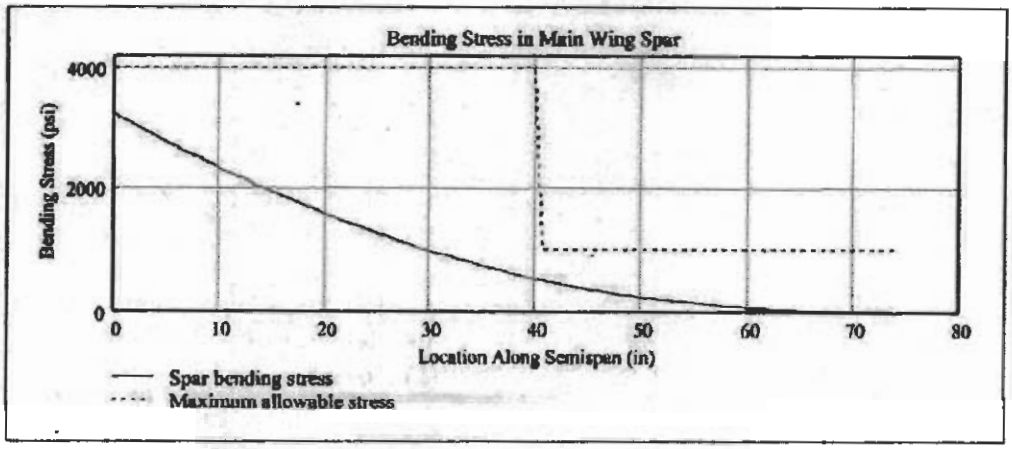

Figure 4.3: Main Spar Bending Stress Using I-Beam

4.3 Weight and Balancing of Aircraft Design

Balancing of the design aircraft was performed along one coordinate axes (longitudinal centerline). The effect of vertical CG location on stability and balance was considered negligible in their overall effect on static stability. The design balance is based on a finite partitioning of the aircraft into thirteen components, each consisting of a respective weight and local CG approximation along the principal axis. This system is further grouped into three subsystems: forward engine compartment, payload, and general structure. The component grouping is shown in Table 4.1. For purposes of balancing, the global system is parameterized around both the engine compartment and payload subsystems while the general assembly is considered static. A two step process is then invoked to statically balance the airplane about the quarter chord of the main wing. This involves movement of the engine compartment first, followed by the payload. The final results of this balancing process are shown in Table 4.1 which shows the respective local CG locations referenced to the main wing quarter chord.

Table 4.1: Design Component Parameters

Component Sub-grouping	Component Name	Local CG Location Relative to Quarter Chord (in)	Component Weight (lbf)
Fwd. Engine Compartment	Engine	-27	1.433
	Nose Landing Gear	-23	0.5
	Fuel Tank	-19	0.3
	Batteries	-14.25	0.25
Payload	Payload	-3.7	31.4
General	Main Landing Gear	7	1.282
	Receiver	0	0.25
	Main Wing	3.7	5.27
	Main Wing Servo's	6.8	0.551
	Fuselage	16.7	0.406
	Vertical Tail	51.5	0.508
	Horizontal Tail	63.8	1.125
	Tail Servo's (2)	65.83	0.551
Total Design Weight:			44 lbf
Overall CG Location:			0 in

4.4 Global CG Location for Off Design Condition

The system balance presented above is performed at design weight (maximum payload), which consequently determines the fixed subsystem positioning. Of equal concern is aircraft performance at payload weights different from those of the design condition. From the standpoint of aircraft balancing, given the set geometry, any additional change in payload weight results in a global CG shift from the initial design parameter. This change, as a function of payload weight, is presented graphically in Figure 4.4 where a coordinate orientation is consistent with that used in Table 4.1.

What Figure 4.4 indicates is an approximate 4 inch aft movement of the global CG at the lowest allowable payload. The neutral point of this design is approximately 5 inches aft of the quarter chord and therefore at minimum payload the aircraft was a 1 inch static margin. In the instance that this does not allow enough margin of static stability for adequate control, consideration is given to moving the light payload forward to shift the CG giving a larger stability margin. This condition is shown as a singular point in Figure 4.4 which corresponds to a six inch forward shift in payload location.

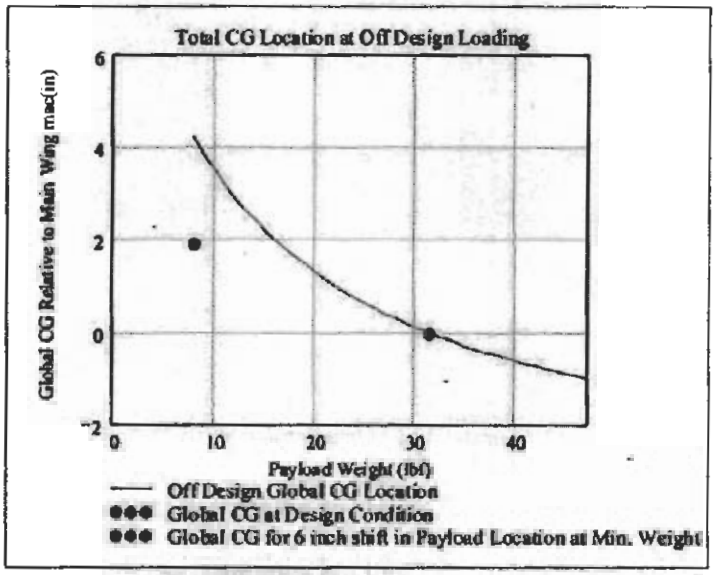

Figure 4.4: Global CG Shift For Off Design Loading Condition

5.0 PROPULSION

The engine for the aircraft is set by the rules committee as an O.S. 0.61 FX Engine with the E-4010 muffler. The engine can not be modified, but the propeller producing the maximum amount of thrust can be chosen. In order to determine the operating characteristics (torque, power, and thrust) of the engine, experimental tests were conducted. The experimental data was corrected to the conditions of a standard day which are 60° F, 29.92 in. of Hg, and dry air. The engine was mounted into a Dyna-Torque test stand to determine the torque at various rpm's. The power the engine produces was calculated from the experimental torque values. Figure 5.1(A) and (B) show the torque and power produced by the engine for a standard day when subjected to different resistances resulting in a range of rpm. The curves in the figures represent a correlation of a theoretical model to the experimental data. This theoretical model was based on manufacturer's specifications and piston engine theory from Heywood[1].

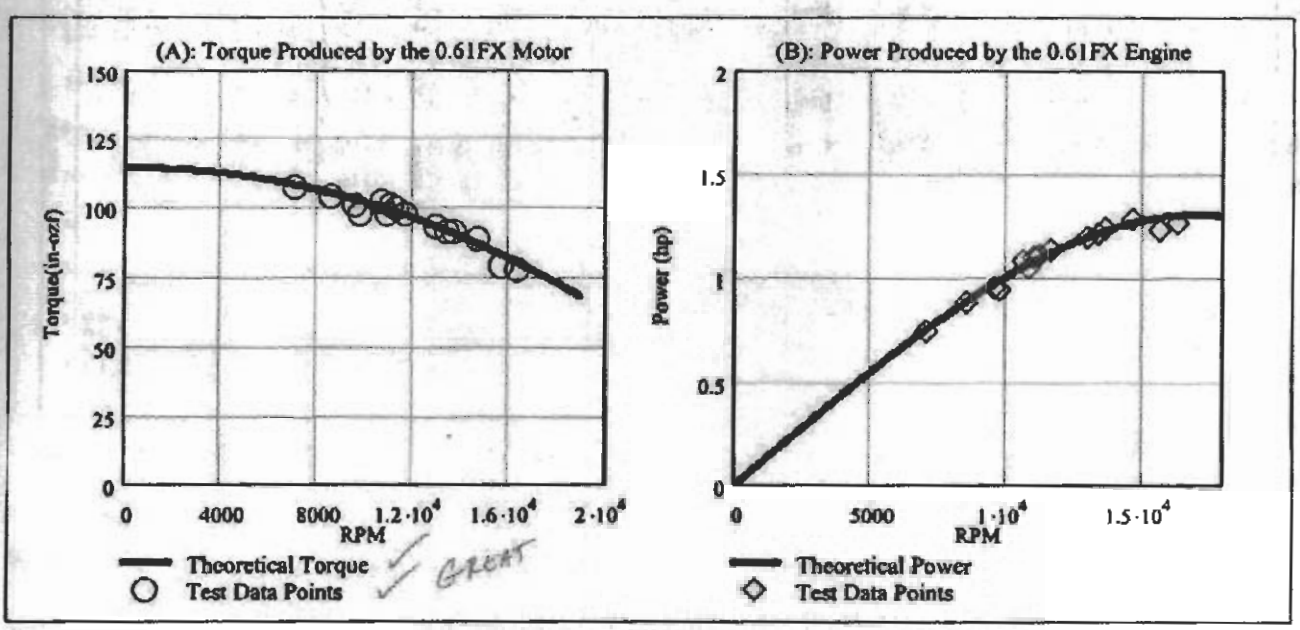

Figure 5.1: Engine Performance Data for (A) Torque (B) Power

Several propellers were tested with the engine to determine the thrust being produced. Fifteen two bladed propellers were tested with the diameters ranging between 11 to 15 inches. The tested propellers were a combination of wood and nylon from several manufacturers. The blade pitch measured at 75%

[1] Heywood, John B., *Internal Combustion Engine Fundamentals*, McGraw-Hill, New York, 1988.

of the radius ($pitch_{75}$) varied for each propeller that was tested. The thrust for each propeller was corrected for a standard day and plotted in Figure 5.2 as a function of rpm. Experimental testing showed the propeller which produced the most thrust was 14 inches in diameter with a 5° $pitch_{75}$ (14x5). The data point corresponding to this propeller is circled in red on the figure. The 14x5 propeller produces 9.14 lbf of thrust at an rpm of 11400. The curves in the figure were calculated using a simple parametric propeller model based on the representative blade theory from Von Mises[2]. Each curve in Figure 5.2 corresponds to a different propeller diameter while any point along a curve is a different representative blade pitch. The representative blade pitch is measured from zero lift. The representative blade pitch of the 14x5 propeller is 12.7°. The model was correlated to match the experimental data for the 14x5 propeller.

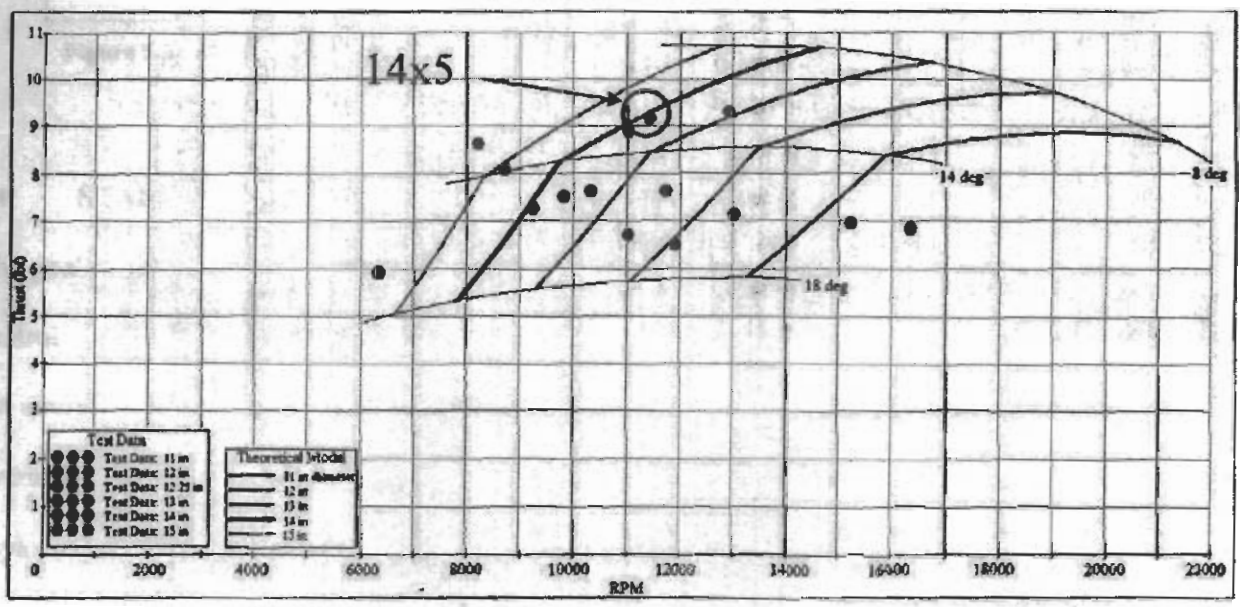

Figure 5.2: Thrust Curves & Test Data Points for Various Propellers

With the models correlated to the test data, the model can be used to determine the rpm that the engine and prop run together using an iterative method. Using the engine and prop matched rpm, the power and thrust the engine and propeller produce together was determined. Figure 5.3 (A) and (B) show these values as functions of velocity. Figure 5.3 (B) shows the thrust at zero flight velocity to be 8.75 lbf. This is slightly less than the thrust test result, displayed in the figure by the red point, since the rpm

[2] Von Mises, Richard, *Theory of Flight by Richard von Mises*, McGraw-Hill Book Company, Inc, New York, London, 1945.

found when matching the engine and prop is 10500. Figure 5.3 (B) also shows that the thrust decreases with increased aircraft velocity. The data produced by Figure 5.3 (A) and (B) was used by the performance group to help determine detrimental flight characteristics.

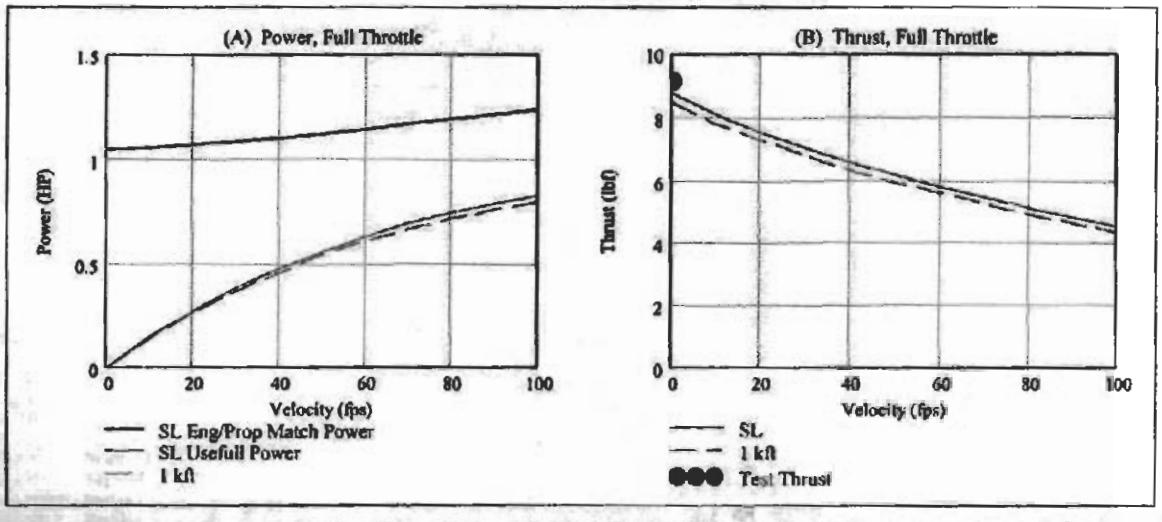

Figure 5.3: (A) Power as a Function of Aircraft Velocity (B) Thrust as a Function of Aircraft Velocity

6.0 STABILITY AND CONTROLS

The goal of the stability and controls group is to calculate the aircraft flight mechanics and construct a control system that enables the aircraft to perform the necessary mission. The operation environment of the aircraft is at low speed, low altitude, and the mission profile requires minimum maneuvering. The aircraft is also required to be easy to control and have robust and predictable pitch stability for different payload configurations.

6.1 Flight Mechanics

The pitch axis is the most important axis under consideration because of the various CG changes, crucial moment arm takeoff roll, and large area of the main wing. Using basic linearized equations of motion, a reasonable horizontal tail coefficient is calculated. Given this coefficient the horizontal tail area was calculated. The elevator size was selected based on common aircraft configurations. An elevator chord fraction of 0.4 and an elevator span fraction of 1.0 were selected. The aircraft static pitching moment

RUDDER – SINCE there is no dihedral angle or effect the rudder will be destabilizing in roll. This will need to be overcome by aileron deflection making coordinated turns difficult. This may be acceptable if the rudder is used primarily for directional control during ground roll only.

balances were also calculated for various flight conditions. Figure 6.1(A) shows the moment coefficient (C_m) as a function of AOA for the design CG, and ± 1.0 inch from the design CG. The neutral point is located approximately 4.5 inches forward of the design CG. Figure 6.1 (B) shows the C_m as a function of AOA for three elevator deflections: 0°, and ± 5°.

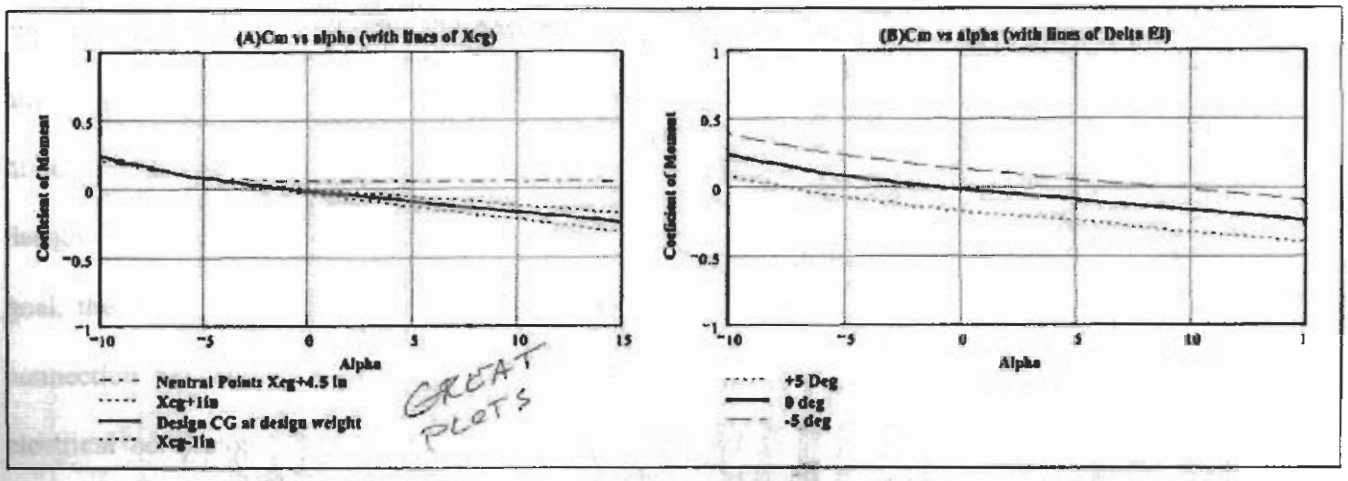

Figure 6.1: Cm for (A) Different CGs, include neutral point, and (B) With various elevator deflections

Yaw axis stability is a primary function of the vertical aerodynamic surface area. Since the fusclage area is relatively small compared to the vertical tail area, only the vertical tail was considered for the yaw stability calculation. Again, a reasonable vertical tail volume coefficient was found and used to calculate the vertical tail side area. The rudder size was also selected based on common aircraft configurations. A rudder chord fraction of 0.4 and a rudder span fraction of 1.0 were selected. Table 6.1 lists the pitch and yaw derivatives for the aircraft configuration.

Table 6.1: Aircraft Control Derivatives

Cm_α	Cm_q	$Cm_{\delta e}$	Cn_β	$Cn_{\delta r}$
-1.128	-12.87	-1.348	0.117	-0.06

Clp Clδa

The main contribution for static stability in the roll axis is the dihedral of the main wing. However, for ease of construction the wing was designed without dihedral. This is feasible considering the flight path involves minimum turning. Both ailerons sizes were selected based on common aircraft configurations. An aileron chord fraction of 0.25 and an aileron span fraction of 0.4 were selected. The roll stability at cruise velocity can be controlled by the pilot deflecting the control surfaces.

I don't agree with this statement. You could argue that the majority of the flight will involve turning.

6.2 Control System

The radio control (RC) control system is built around a Futaba 9CAP controller and receiver unit. The size of the aircraft poses a special challenge to the servo system. Separate servos were chosen for the left and right ailerons to eliminate long control linkages. Again, for similar reasons and ease of construction, separate servos for the nose wheel and rudder were also selected. The large size of the aircraft configuration and limited space for transportation to the flight-line required the aircraft to be divided into several separate segments. Due to the separate segments, a control and linkage system design is needed to limit the field work necessary to assemble the aircraft for flight. To achieve this goal, the servo and control surface linkages are self contained in each segment. The only physical connection between the control system and the major segments are servo electrical wires. With electrical connectors placed at the breaks between segments, the flight-line assembly work for the control system is simplified to connecting electrical wires.

The forward fuselage contains the receiver, the battery pack, the nose gear servo, and engine throttle servo. The left and right outer taper sections of the wing contain the servo for their respective ailerons. The rear fuselage contains the rudder and elevator servos. In order to have the most robust and rigid control linkage possible, the four main control surfaces (left and right ailerons, elevators and rudder) are all each connected to their respective servos using "horn" linkages and short rigid push rods. This arrangement is typically found on aileron linkages for smaller RC aircraft. The nose wheel and throttle are controlled using flexible rod linkages.

7.0 PERFORMANCE

Aircraft performanee characteristics were calculated to ensure a successful completion of the mission. One such calculation was the determination of drag and thrust as a function of velocity at flight conditions. The aerodynamics group provided the trimmed aircraft drag polar while thrust as a function of velocity was calculated by the propulsion group. The thrust values are plotted at sea level and 1000 ft

in Figure 7.1 (A). The drag values are also plotted in Figure 7.1 (A) for the design weight (solid red line) as well as the design weight ± 10 lbf (dashed and dotted red lines). For the configuration, the thrust is equal to the drag at a speed of 73 feet per second (fps), indicating the maximum aircraft speed. The thrust and drag for takeoff conditions, shown in Figure 7.1 (B), were determined by adding the frictional rolling losses of the landing gear wheels.

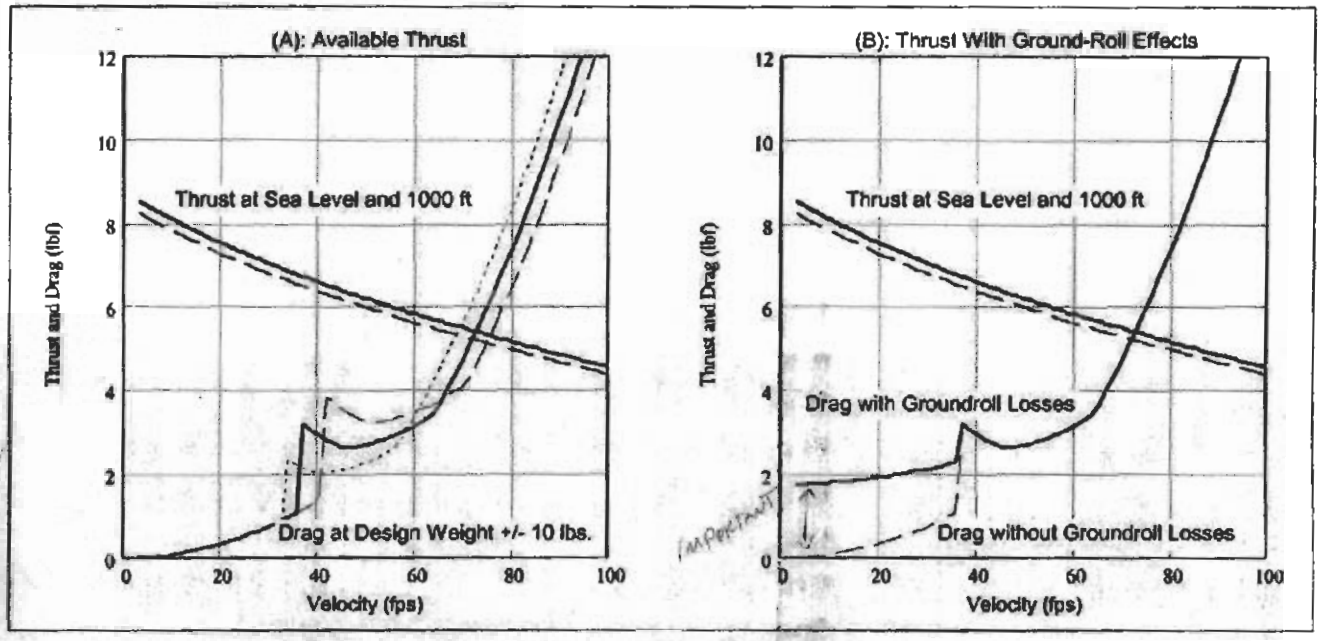

Figure 7.1: Thrust and Drag Without & With Rolling Losses

The velocity needed for takeoff is plotted for three different design weights in Figure 7.2. Again, the solid line represents the design weight while the dashed and dotted lines represent the design weight ±10lbf. Using Figure 7.2, the speed needed for take-off was determined to be approximately 37 fps.

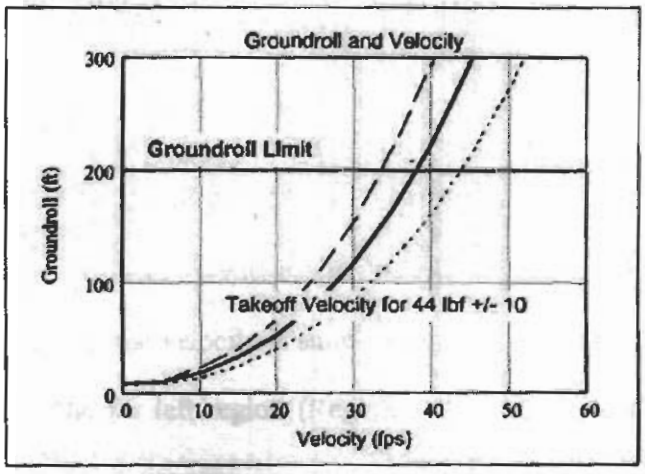

Figure 7.2: Takeoff Velocity

Figure 7.3 (A) and (B) are plots of the rate and angle of climb as a function of velocity. These functions are plotted for steady state, sea level standard conditions with a full throttle setting. The velocities for the max rate of climb and max angle of climb are shown in Figure 7.3 (A) and (B). Figure 7.4 is a V-N diagram showing the g-forces the aircraft structure experiences throughout the flight regime at design weight and design weight ±10lbf.

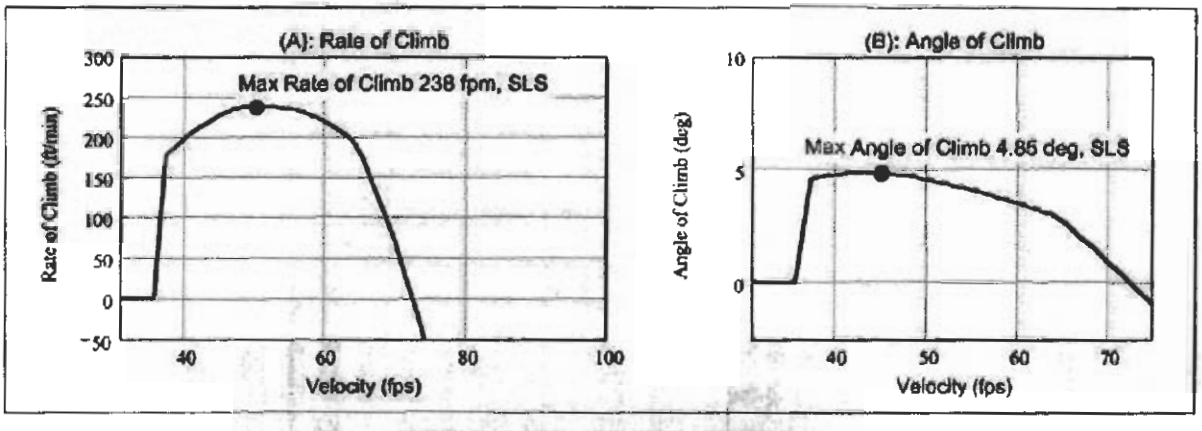

Figure 7.3: Rate and Angle of Climb

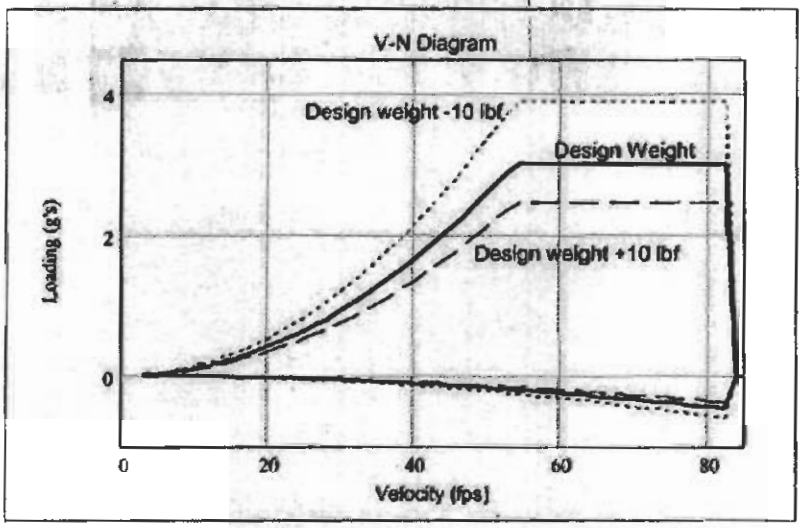

Figure 7.4: V-N Diagram

The turning radius versus aircraft velocity was calculated to determine if the wing will stall or break. The turning radius as a function of the velocity is shown in Figure 7.5. Three flight regions can be seen separated by the solid line. The far left region (Region 1) represents flight conditions which would

cause the wing to stall. The far right region (Region 3) represents flight conditions which would cause the wing spar to break. Sustainable flight is possible only in Region 2.

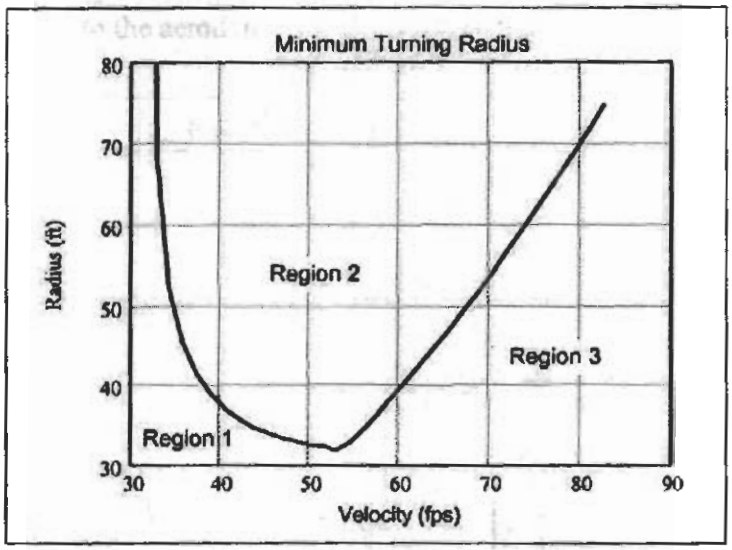

Figure 7.5: Turning Radius

8.0 TRADE STUDY

A trade-off study is conducted with the aim of maximizing the payload capacity of the aircraft. Given that the takeoff characteristics of the aircraft can be calculated via the performance model, one can optimize the aircraft geometry in order to maximize the payload weight. The optimization process is constrained such that the vehicle must have specific takeoff characteristics. In particular, it must have a ground roll distance of 190 ft, which is 10 ft short of the competition limit, providing a reasonable margin of error. The vehicle must also liftoff with a climb rate of 180 ft/min, a rate sufficient to sustain climb in the presence of significant adverse perturbations. The dimensions of the wing are varied in order to find viable configurations which meet these constraints. Consequently, as the wing dimensions increase, so does the total weight of the wing. Given that the wing composes over 50% of the empty weight, as shown in Table 4.1, the payload capacity will be limited largely by the wing dimensions.

The optimization process is iterated on the design weight, or total weight including payload. For each iteration, the design weight is set and then the wing span and wing area are varied in order to meet the aforementioned takeoff constraints. While each parameter has an effect on the ground roll and climb

rate, the wing span and area are highly correlated and orthogonal to each other. The ground roll distance is inversely proportional to the induced drag, which is dominated by the wing span. Similarly, the lift off climb rate is proportional to the aerodynamic lift, which is highly correlated to the wing area.

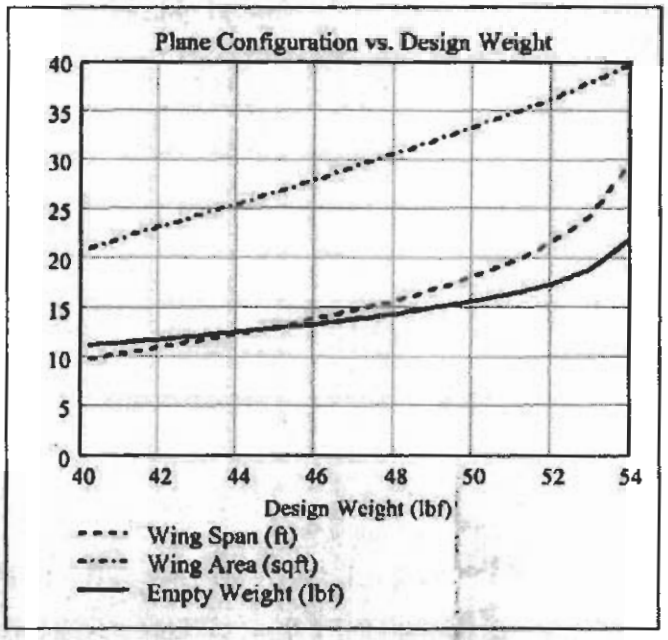

Figure 8.1: Trade Study of Aircraft Geometry

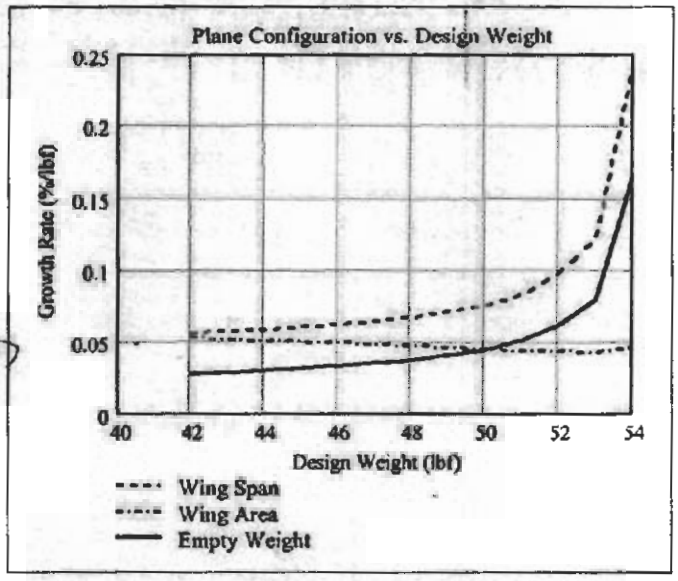

Figure 8.2: Trade Study of Geometry Growth Rates

The geometry variables for viable configurations as a function of design weight are shown in Figure 8.1 and the corresponding growth rates are shown in Figure 8.2. Note the growth rate in the dimensions of the aircraft configuration as the design weight increases above 50 lbf.

Once the viable geometry for a given design weight is determined, the required structure is calculated via the structures model, resulting in a predicted empty weight of the aircraft. Subtracting this empty weight of the aircraft from the design weight gives the maximum payload weight capacity of the configuration. The resulting relationship between the design weight and the payload capacity is shown in Figure 8.3. Viable configurations are termed as those which would exhibit the takeoff characteristics as previously outlined. The parameters of the three specific configurations in Figure 8.3 are tabulated in Table 8.1.

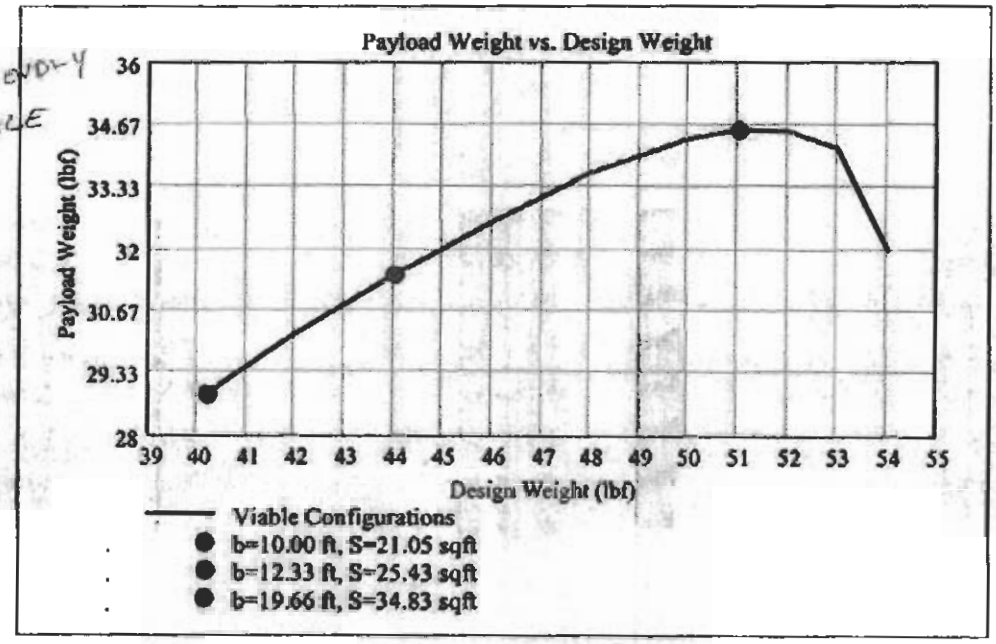

Figure 8.3: Trade Study of Payload Capacity and Design Weight

Table 8.1: Comparison of Viable Configurations

Design Weight [lbf]	40.20	44.00	51.00
Wing Span [ft]	10.00	12.33	19.66
Wing Area [sqft]	21.05	25.43	34.83
Empty Weight [lbf]	11.32	12.58	16.47
Payload Capacity [lbf]	28.87	31.42	34.53
Wing Span Decrease from Optimum [%]	49.1	37.3	-
Wing Area Decrease from Optimum [%]	39.6	27.0	-
Empty Weight Decrease from Optimum [%]	31.2	23.6	-
Payload Capacity Decrease from Optimum [%]	16.4	9.0	-

Note the maximum payload capacity is at a design weight of 51 lbf, indicated by the red marker, which roughly corresponds to the aforementioned sharp rise in dimensions. This optimum configuration corresponds to a wingspan of almost 20 ft and a wing area of 35 ft^2. Heuristically, this seems excessive from the standpoint of resources and construction capacity. It is also apparent from the plot that if the design weight exceeds the optimum, the payload capacity drops extremely fast. Expecting a reasonable amount of error in the analytical model, vehicle construction, and environmental perturbations, perhaps 10% or more, it becomes obvious that one would be safer in choosing a more conservative design weight. Choosing a design weight of 44 lbf yields a configuration with a significantly reduced wing span, wing area, and empty weight with only a 9% reduction in payload capacity, as shown in Table 8.1. Considering the design with a 10 ft wingspan, the competition minimum, the wing dimensions are similarly reduced, but this results in a non-proportional 16% reduction in payload capacity. Thus, the configuration corresponding to the design weight of 44 lbf is chosen as the most logical design.

Good Reasoning.
Excellent Analysis.

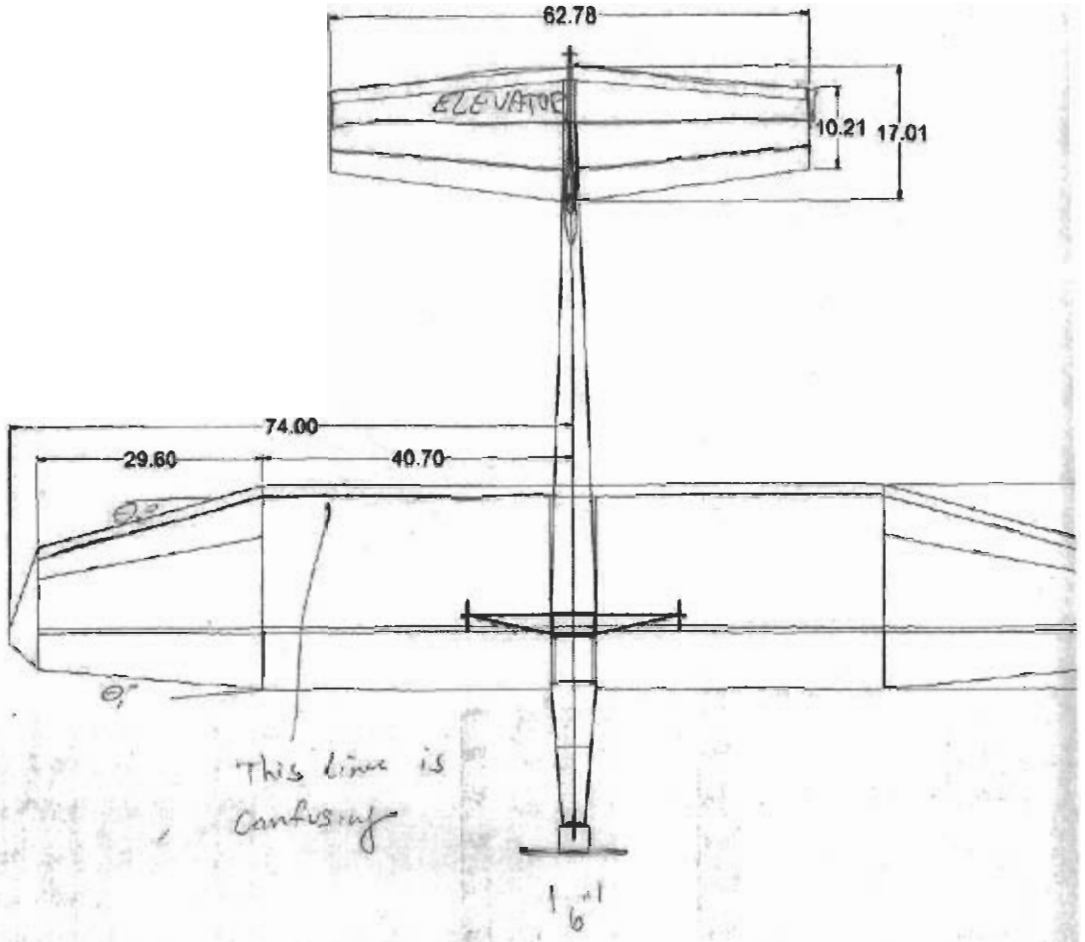

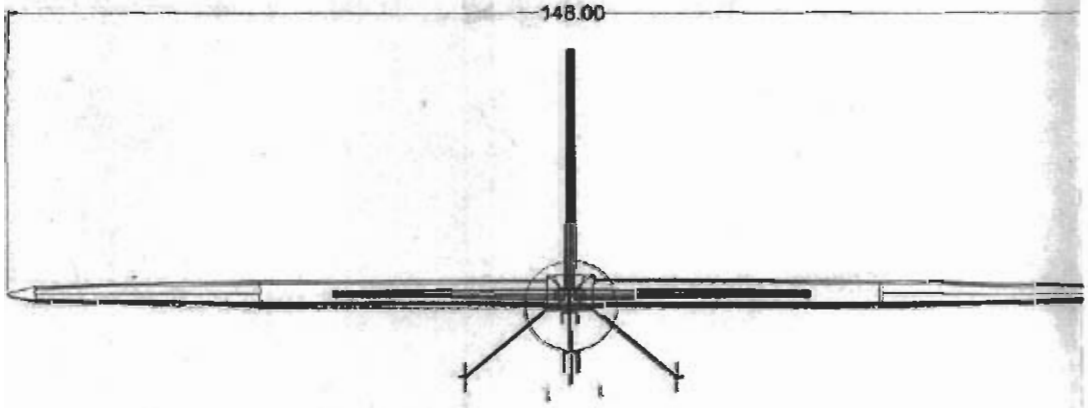

Other supplemental dimensions could include

l_{HT}

l_{VT}

CG RANGE

AC

MAC

Roll, TIP BACK ANGLE

ALSO NICE WOULD BE % Static Pitch Margin VS Payload Weight TABLE.

Area Data	
Part Description	Area (sq. in.)
Forward Fuse	1270.85
Rear Fuse	1785.69
Horiz. Tail	1689.70
Vert. Tail	808.68
Landing Gear	145.86
Wing	8185.29
Total Area	13886.07

Looks like you calculated Swet instead of planform area.

Wing Span	148.00 inches
Fuse Length	103.40 inches
Wing Airfoil	DAE 11
Aspect Ratio	6

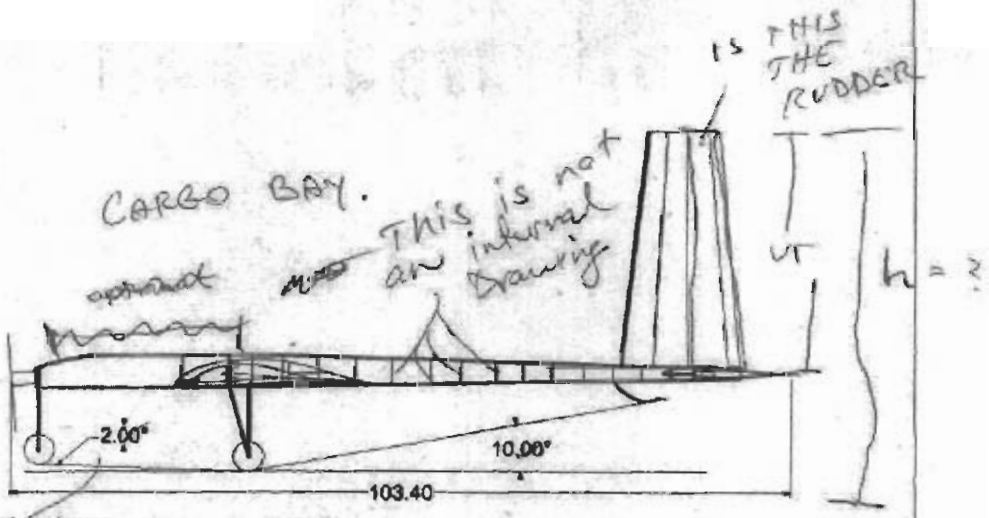

Don't NEED THIS ACCURATELY

Team # 029 University of Cincinnati AeroNatiCats			
3-View of Overall Aircraft			
Size B	All Dimensions are in inches unless other wise noted.	DWG NO. UCANC04	REV A
DWG BY: L. Kramer		SHEET 1 of 5	

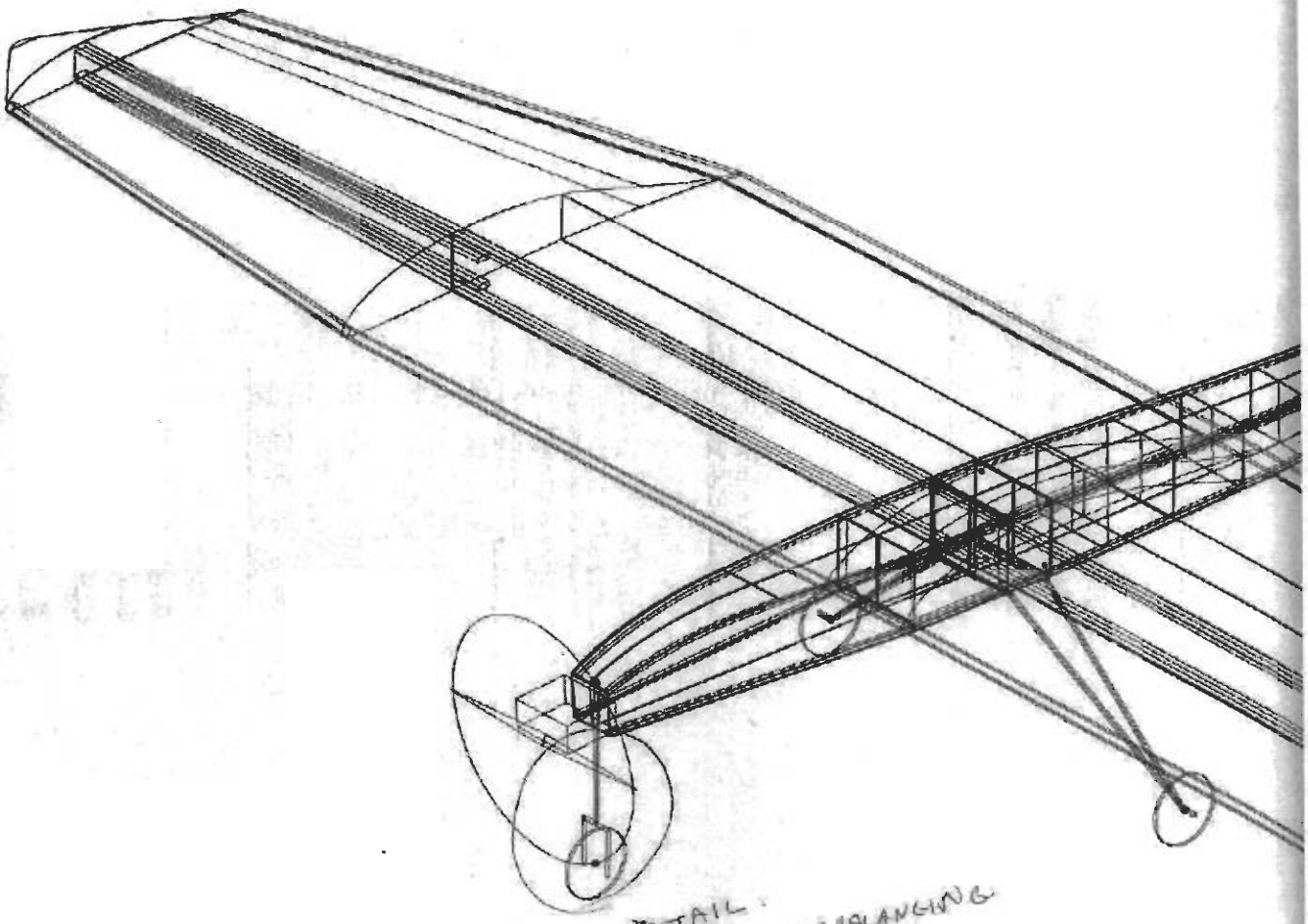

DETAIL.
THIS IS A BALANCING
INTERFACE.

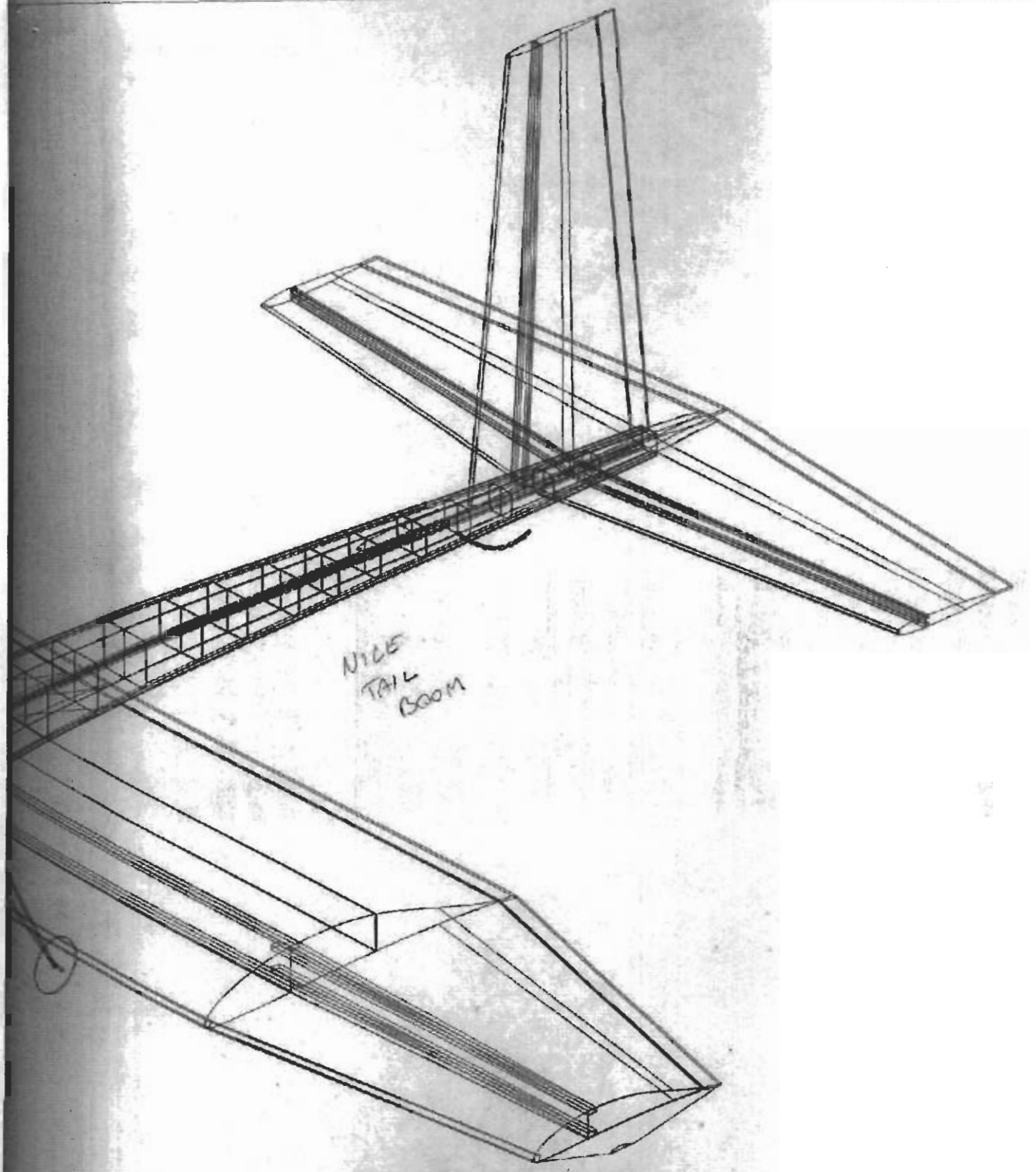

Team # 029 University of Cincinnati AeroNatiCats			
Isometric View of Aircraft			
Size B	All Dimensions are in inches unless other wise noted.	DWG NO. UCANC04	REV A
DWG BY: L. Kramer		SHEET 2 of 5	

Tip Chord & Root Chord of AIL ?

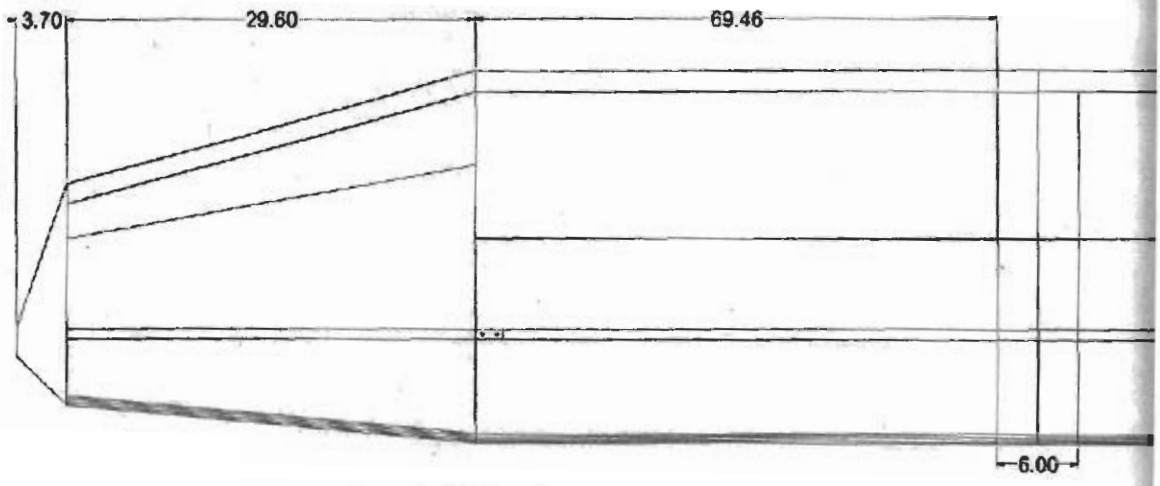

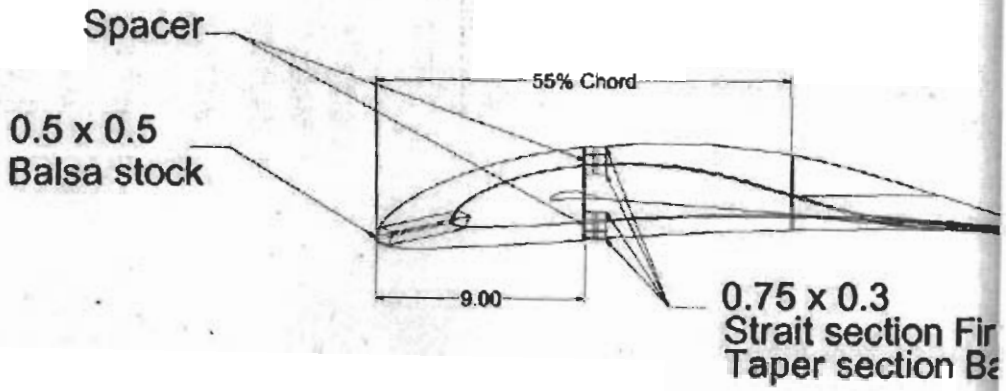

DAE 11 Airfoil

Notes: D spar shear web is 1/16 plywood
D spar sheeting 1/64 plywood
55% shear web is 1/16 Balsa
Rib cap strips 1/16 Balsa

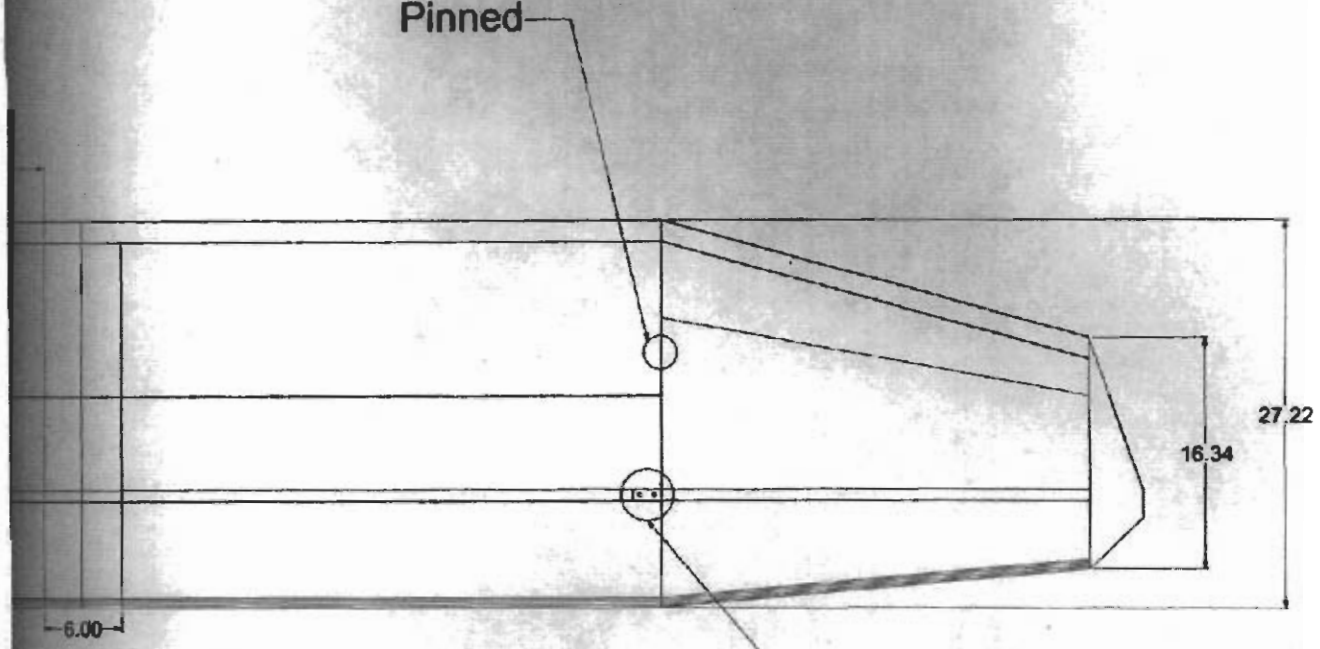

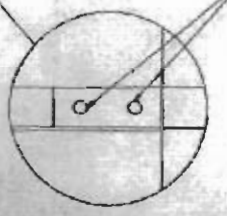

Taper section mount

0.3
section Fir Stock
section Balsa Stock

Airfoil

Team # 029 University of Cincinnati AeroNatiCats			
Wing Detail DAE 11			
Size B	All Dimensions are in inches unless other wise noted.	DWG NO. UCANC04	REV A
DWG BY: L. Kramer		SHEET 3 of 5	

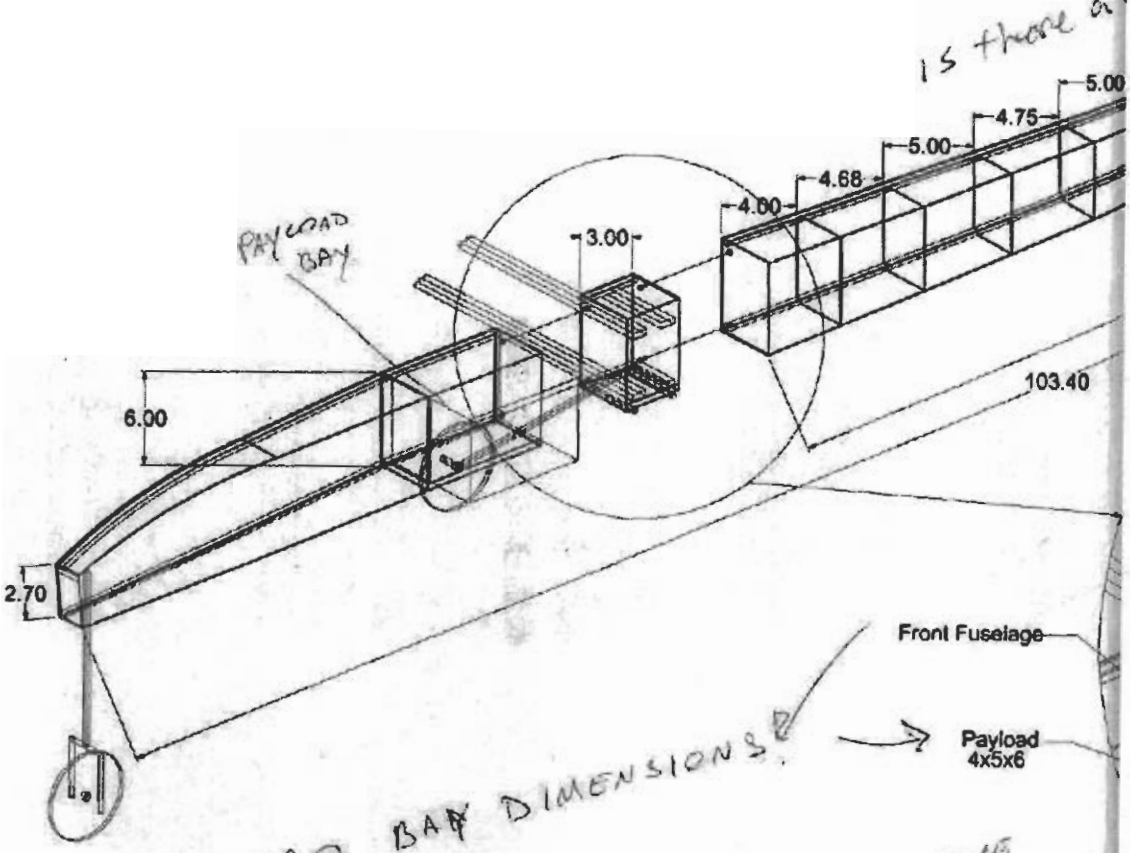

Is there a

· CARGO BAY DIMENSIONS?

not complete.

ACCESS

I FIND THE HALF FUSE CONFUSING.

Note: Dimensions for half fuselage

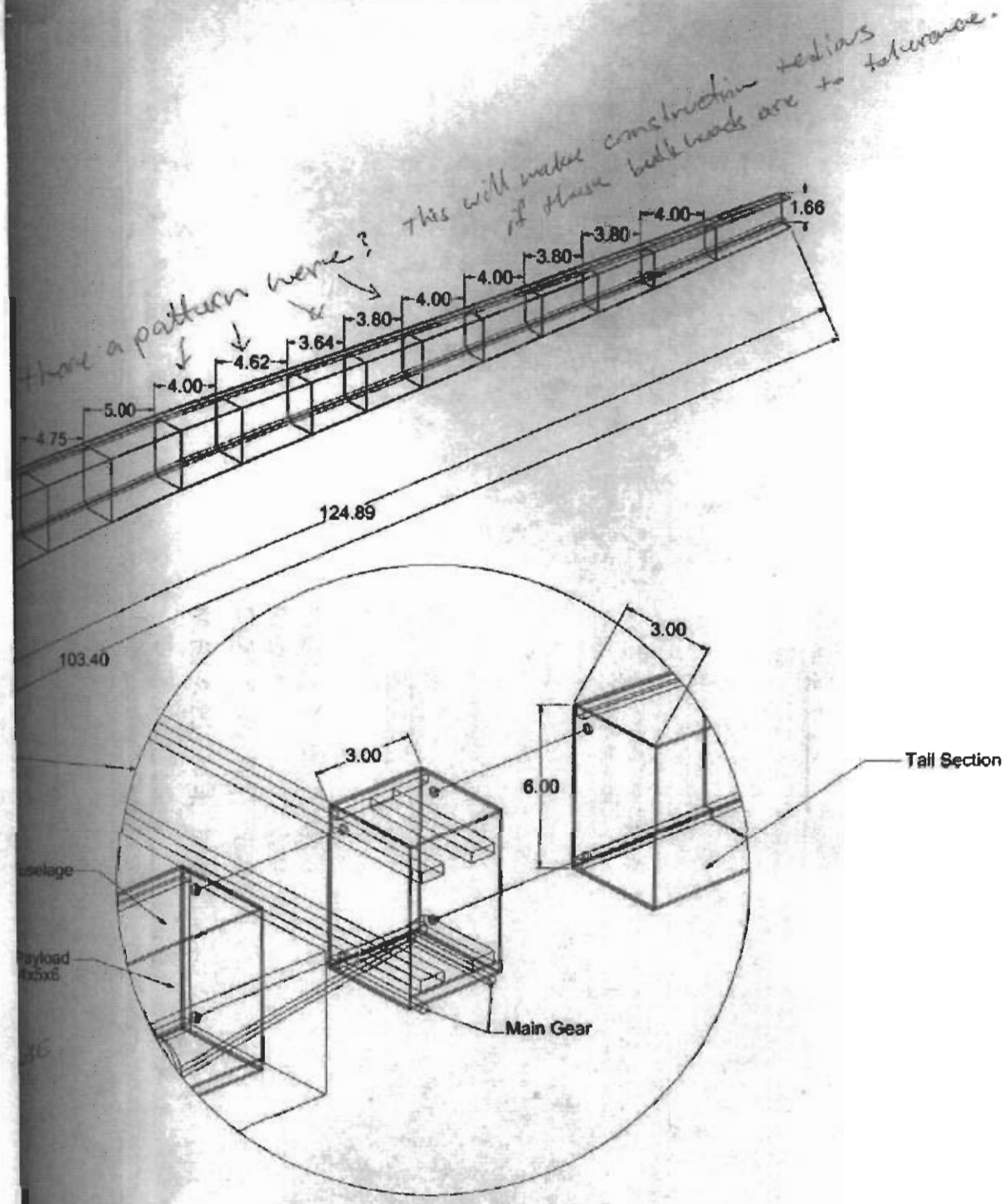

Team # 029 University of Cincinnati AeroNatiCats			
½ Fuselage Detail			
Size B	All Dimensions are in inches unless other wise noted.	DWG NO. UCANC04	REV A
DWG BY: L. Kramer		SHEET 4 of 5	

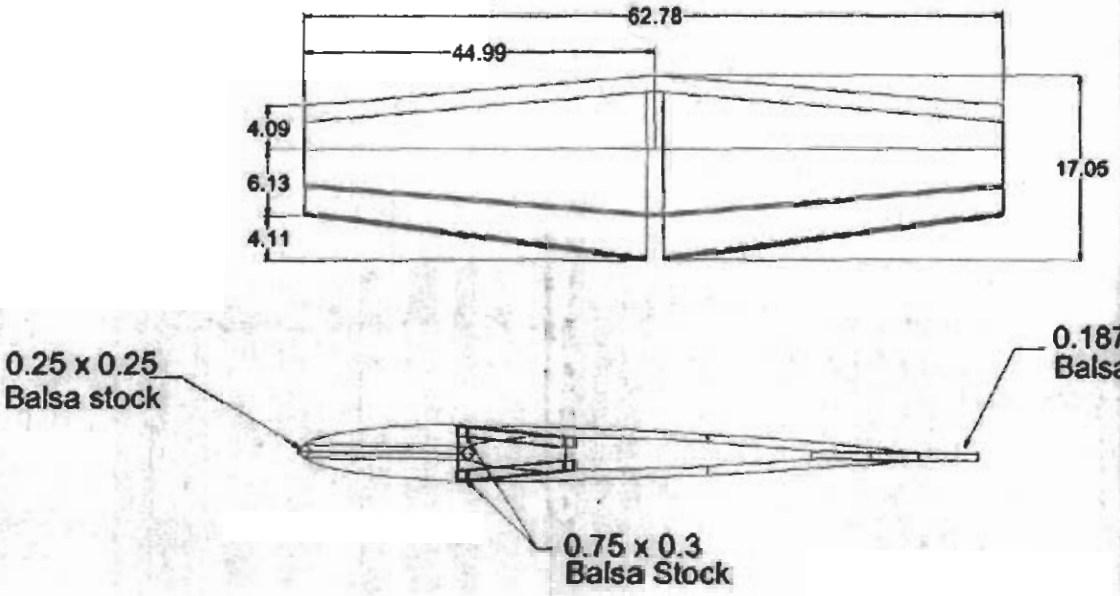

NACA 0009 Airfoil

Notes: D spar shear web is 1/16 plywood
D spar sheeting 1/64 plywood
Rib cap strips 1/16 Balsa

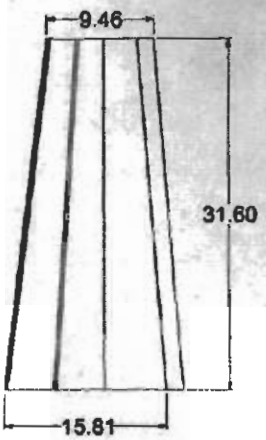

17.05

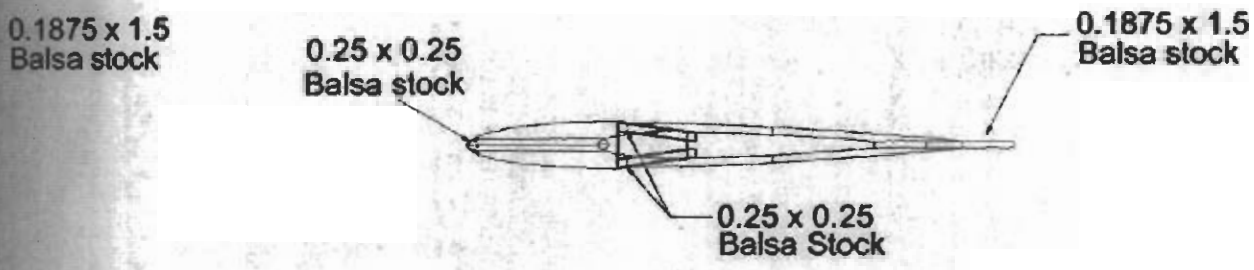

NACA 0009 Airfoil

Team # 029 University of Cincinnati AeroNatiCats			
Tail Detail NACA 0009			
Size B	All Dimensions are in inches unless other wise noted.	DWG NO. UCANC04	REV A
DWG BY: L. Kramer		SHEET 5 of 5	

AeroNatiCats, University of Cincinnati

Predicted Payload Weight vs. Density Altitude

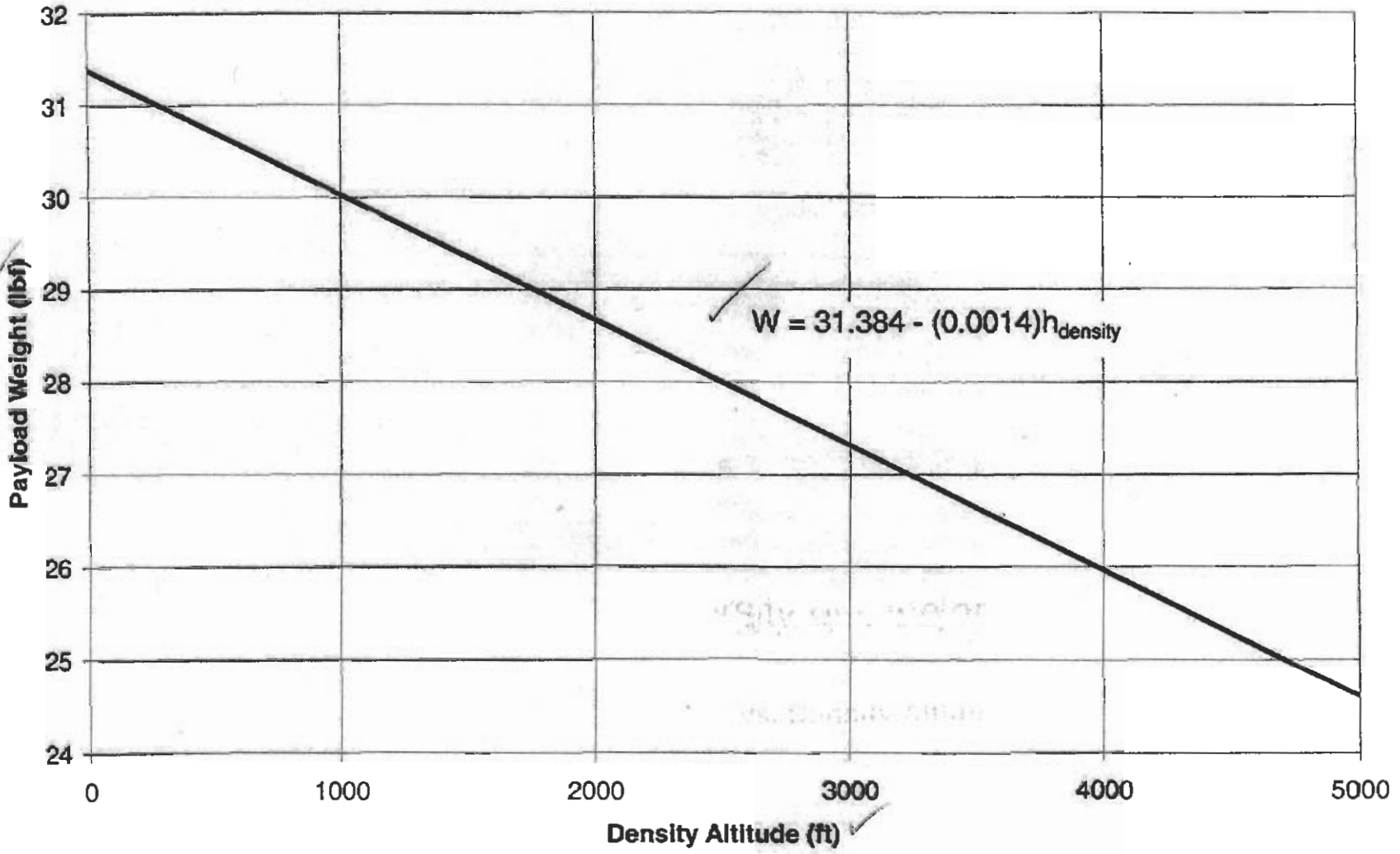

Team Number 029

SAE Aero Design Report Scoring Worksheet

Judge Initials: CWD 2

School Name:	University Of Cincinnati	Class:	Regular
Team Name:	AeroNatiCats	Team #:	29

Design Report (Max Score 30):		Points	Awarded	Score: 28.85
	RECORD ALL SCORES ROUNDING TO 2 DECIMAL PLACES			Score =Total Points / 10
Format Requirements		20.00	20.00	
	Team and School Name and Team number on Title page Bound Report, 8 1/2" X 11" paper, 25 Page Max (excluding plans). 12 point font Min, 1"X1"X1/2"X1/2" Margins Min			
Design Process	(Research, Concept, Methodology, Procedure)	50.00	49.00	
Payload Prediction	(Calculations / Description)	80.00	79.00	
Performance, Stability, & Control	(Calculations / Description)	50.00	48.50	
Innovation	(Design, Materials, Construction)	50.00	42.00	
Clarity / Organization		30.00	30.00	
Grammar / Punctuation / Spelling		20.00	20.00	

28.175

Design Plans (Max Score 30):		Points	Awarded	Score: 21.50
				Score =Total Points /
Plan Format Requirements		20.00	20.00	
	11" X 17" paper foldouts, 5 Page Max, Bound in Report Team number on all pages English or SI units used			
3 View Sheet		100.00	70.00	
	Aeronautical format 3 view Major component dimensions and planform areas given Cargo bay volume data given			
Plan Sheets		60.00	60.00	
	Cargo bay and other appropriate dimensions given			
Clarity		50.00	40.00	
Detail		50.00	25.00	

22.7

Payload Prediction Graph (Max Score 10):		Points	Awarded	Score: 10.00
				Score =Total Points / 10
Graph Format		30.00	30.00	
	Team and School Names on top, Team number bottom right 8 1/2" X 11" paper, 1 page Max, NOT bound to report Landscape format Axis units X = feet Y = lbs			
Linear Equation Given		30.00	30.00	
Readability of Grid		20.00	20.00	
	Sufficient lines Clear engineering axis divisions (ie 1, 2 ,5, 10,...) Clarity			
Visual Presentation		20.00	20.00	

9.7